

# RSC Advances



This is an *Accepted Manuscript*, which has been through the Royal Society of Chemistry peer review process and has been accepted for publication.

*Accepted Manuscripts* are published online shortly after acceptance, before technical editing, formatting and proof reading. Using this free service, authors can make their results available to the community, in citable form, before we publish the edited article. This *Accepted Manuscript* will be replaced by the edited, formatted and paginated article as soon as this is available.

You can find more information about *Accepted Manuscripts* in the [Information for Authors](#).

Please note that technical editing may introduce minor changes to the text and/or graphics, which may alter content. The journal's standard [Terms & Conditions](#) and the [Ethical guidelines](#) still apply. In no event shall the Royal Society of Chemistry be held responsible for any errors or omissions in this *Accepted Manuscript* or any consequences arising from the use of any information it contains.

# Facile synthesis of porous Li-rich layered $\text{Li}[\text{Li}_{0.2}\text{Mn}_{0.534}\text{Ni}_{0.133}\text{Co}_{0.133}]\text{O}_2$ as high-performance cathode materials for Li-ion batteries

Chenwei Cao<sup>a</sup>, Liujiang Xi<sup>ab</sup>, Kwan Lan Leung<sup>a</sup>, Man Wang<sup>a</sup>, Ying Liu<sup>a</sup>, Ruguang Ma<sup>a</sup>, Shiliu Yang<sup>a</sup>, Zhouguang Lu<sup>\*c</sup> and C. Y. Chung<sup>\*a</sup>

Received (in XXX, XXX) Xth XXXXXXXXXX 20XX, Accepted Xth XXXXXXXXXX 20XX

DOI: 10.1039/b000000x

Lithium-rich layered metal oxides have drawn much recent attention due to their high rechargeable capacity of 250-300 mAh g<sup>-1</sup>. Herein, we report the synthesis of porous  $\text{Li}[\text{Li}_{0.2}\text{Mn}_{0.534}\text{Ni}_{0.133}\text{Co}_{0.133}]\text{O}_2$  metal oxide powders using a facile polymer-thermolysis method. X-ray powder diffractometry (XRD) results show that a well-crystallized layered structure was obtained when the calcination temperatures reach 800 °C. Pores in the range of 100-200 nm are observed using scanning electron microscopy (SEM). The porous  $\text{Li}[\text{Li}_{0.2}\text{Mn}_{0.534}\text{Ni}_{0.133}\text{Co}_{0.133}]\text{O}_2$  synthesized at 850 °C shows much superior electrochemical performance to the sample synthesized by the traditional coprecipitation-calcination method, with a high initial coulombic efficiency of 87% and initial discharge capacity of 245.4 mAh g<sup>-1</sup> at 15 mA g<sup>-1</sup> in the voltage window 2-4.6 V. A capacity retention of 81% was obtained after 300 cycles at 300 mA g<sup>-1</sup>. The higher capacity and improved rate performance of porous  $\text{Li}[\text{Li}_{0.2}\text{Mn}_{0.534}\text{Ni}_{0.133}\text{Co}_{0.133}]\text{O}_2$  can be predominantly attributed to enhanced Li<sup>+</sup> intercalation kinetics resulting from the highly porous structure.

## Introduction

Driven by the success of Li-ion batteries (LIBs) in the portable electronic market and the global resolution to reduce fossil fuels usage, considerable efforts are being paid to extend the use of LIBs in electrical vehicles (EVs), hybrid electrical vehicles (HEVs) and smart grids<sup>1,2</sup>. However, current commercial cathode materials such as layered  $\text{LiCoO}_2$ ,  $\text{LiNi}_{0.8}\text{Co}_{0.15}\text{Al}_{0.05}\text{O}_2$ ,  $\text{LiNi}_{0.33}\text{Co}_{0.33}\text{Mn}_{0.33}\text{O}_2$ , spinel  $\text{LiMn}_2\text{O}_4$ , and olivine  $\text{LiFePO}_4$  only have capacities around 120–200 mAh g<sup>-1</sup>, which are insufficient to meet the requirements for EV and HEV applications<sup>3–5</sup>. Therefore, it is of great importance to develop new high-energy and high-power cathode materials<sup>6–9</sup>.

Commonly denoted as  $x\text{Li}_2\text{MnO}_3 \cdot (1-x)\text{LiMO}_2$  (M = Mn, Ni, Co, etc.), the lithium-rich layered metal oxides (LLOs) have attracted much attention in recent years, thanks to its high rechargeable capacity of 250-300 mAh g<sup>-1</sup>, low cost, and superior safety characteristics<sup>10–12</sup>. The LLOs can be considered as a composite of layered  $\text{LiMO}_2$  and layered  $\text{Li}_2\text{MnO}_3$  (or  $\text{Li}(\text{Li}_{1/3}\text{Mn}_{2/3})\text{O}_2$ ), which have very similar crystal structure and can form a homogeneous solid solution. The high capacity of LLOs originates from the activation of the  $\text{Li}_2\text{MnO}_3$  component when charged above 4.4~4.5 V, which transforms into electrochemically active  $\text{MnO}_2$  and improves the structural stability during cycling at the same time<sup>13–16</sup>.

Nonetheless, rate performance of the lithium-rich layer oxides is still unsatisfying due to the material's sluggish kinetics and low conductivity<sup>17–20</sup>. Various techniques, including coprecipitation-calcination method<sup>21–23</sup>, sol-gel process<sup>24–26</sup>, molten salt method<sup>27</sup> and combustion synthesis<sup>28,29</sup> have been used to synthesize LLOs. In this study, we adopted a one-step polymer-thermolysis method to prepare LLOs. Variations of this method have been reported by Das et al.<sup>30</sup>, He et al.<sup>31</sup> and Jiang et al.<sup>32</sup> for the synthesis of nanocrystalline ceramics and LLOs.

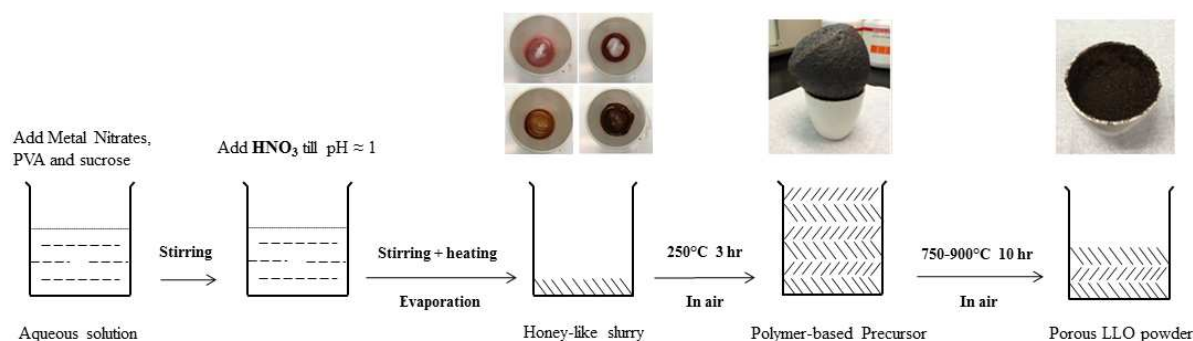
Compared with other fabrication methods, the polymer-

thermolysis method can produce products with good chemical homogeneity, less agglomeration, and most importantly, porous structure formed during the thermolysis process. For example, using a similar method, Jiang et al.<sup>32</sup> has fabricated mesoporous  $0.4\text{Li}_2\text{MnO}_3 \cdot 0.6\text{LiNi}_{2/3}\text{Mn}_{1/3}\text{O}_2$  with a pore diameter of ca. 3 nm with excellent electrochemical performance. The porous structure is desirable for electrochemical applications as it creates a larger contact area between the electrode material and the electrolyte, leading to enhanced lithium diffusion and hence improving the electrochemical performance.

## Experimental Section

### Synthesis of porous $\text{Li}[\text{Li}_{0.2}\text{Mn}_{0.534}\text{Ni}_{0.133}\text{Co}_{0.133}]\text{O}_2$ using polymer-thermolysis (PT) method

The typical polymer-thermolysis (PT) procedure is illustrated in Scheme 1. To obtain the polymer-based precursor, firstly an aqueous solution containing stoichiometric amounts of manganese, nickel, cobalt and lithium (with 5 at.% excess) nitrates was thoroughly mixed with aqueous solutions of polyvinyl alcohol (PVA) and sucrose under magnetic stirring. The molar ratio of the metal ions, PVA monomer units and sucrose was fixed at 1:0.05:2. The pH was adjusted to 1 by adding nitric acid. Then the above solution was gently heated on a hotplate until a honey-like slurry was formed. Afterwards, the slurry was slowly heated up to 250 °C in air, transforming into a fluffy voluminous carbonaceous mass, taken as the precursor. Finally, the fluffy polymer-based precursor was crushed and calcined separately at 750 °C, 800 °C, 850 °C and 900 °C for 10 hours in air. After natural cooling, the porous  $\text{Li}[\text{Li}_{0.2}\text{Mn}_{0.534}\text{Ni}_{0.133}\text{Co}_{0.133}]\text{O}_2$  layered oxide powders were obtained. For the ease of later discussion, the samples calcined at 750 °C, 800 °C, 850 °C and 900 °C were denoted as PT-750, PT-800, PT-850 and PT-900, respectively.



**Scheme 1** Schematic illustration of the polymer-thermolysis method for the preparation of porous LLO.

### Synthesis of $\text{Li}[\text{Li}_{0.2}\text{Mn}_{0.534}\text{Ni}_{0.133}\text{Co}_{0.133}]\text{O}_2$ particles using coprecipitation-calcination (CP) Method

For comparison, the  $\text{Li}[\text{Li}_{0.2}\text{Mn}_{0.534}\text{Ni}_{0.133}\text{Co}_{0.133}]\text{O}_2$  layered oxides were also synthesized through a two-step coprecipitation-calcination (CP) method. Transition metal hydroxide precipitates were obtained by mixing the aqueous solutions of metal nitrates and sodium hydroxide under vigorous stirring. The concentration of the solutions was 2M. The pH was controlled at approximate 10~11. The precipitates were collected by centrifugation and dried in a vacuum chamber at 80 °C for 12 h. In the second step, the metal hydroxides and lithium hydroxide in a molar ratio of 0.8:(1.2\*1.05) were thoroughly mixed by grinding and then calcined at 850°C in air for 10 h. After cooling, a grayish oxide power was obtained. This sample is labelled as CP-850.

### Structural and morphological characterizations

To study the crystalline structures of the as-prepared powders, X-ray diffraction (XRD) patterns in the  $2\theta$  range of 10-80° were collected using a Philips X'Pert MRD X-ray diffractometer with a Cu  $K\alpha$  radiation operated at 40 kV and 30 mA. The morphologies and elemental distribution of the powders were examined with a scanning electron microscope (SEM, JEOL-820) equipped with energy-dispersive X-ray spectroscopy (EDS), a field-emission SEM (Hitachi S4800) and a transmission electron microscope (TEM, CM200 FEG operated at 200 kV). Thermogravimetric analysis (TGA) was performed under oxygen atmosphere in the temperature range of 20-850 °C with a Universal V4.5A TA Instrument. The Brunauer-Emmett-Teller (BET) specific surface areas of the powders were measured from the  $\text{N}_2$  adsorption/desorption isotherms using a NOVA 1200e Surface Area and Pore Size Analyzer (Quantachrome Instruments).

### Electrochemical Characterization

The electrochemical properties of the as-prepared  $\text{Li}[\text{Li}_{0.2}\text{Mn}_{0.534}\text{Ni}_{0.133}\text{Co}_{0.133}]\text{O}_2$  powders as cathode materials were analyzed using CR2032 coin-type half-cells. The cathode slurry was prepared by mixing  $\text{Li}[\text{Li}_{0.2}\text{Mn}_{0.534}\text{Ni}_{0.133}\text{Co}_{0.133}]\text{O}_2$  powders, acetylene black, and polyvinylidene fluoride (PVDF) binder in an 8:1:1 weight ratio, using N-Methyl pyrrolidone (NMP) as solvent. The slurry was then casted onto an aluminum foil and dried at 110 °C for 12 h in a vacuum oven. Circular

cathode discs were punched out from the aluminum foil. The mass of active material on each cathode disc was approximately 2 mg. The testing cells were assembled in a controlled glove box filled with Argon gas, using lithium metal as the counter electrode, a layer of Celgard 2032 (Celgard, Inc., USA) as the separator, and an electrolyte composed of 1M lithium hexafluorophosphate ( $\text{LiPF}_6$ ) dissolved in ethylene carbonate (EC) and dimethylcarbonate (DMC) (1:1 in volume). The fresh-assembled cells were rested for 5 hours before testing. Galvanostatic discharge-charge tests were carried out at room temperature with an Arbin Testing Workstation (BT 2000, College Station, Texas, USA). The cells were cycled in the voltage range 2–4.6 V (vs.  $\text{Li}^+/\text{Li}$ ) at different current densities from 0.05 to 10C (1C rate corresponds to a current density of 300  $\text{mA g}^{-1}$ ). Cyclic voltammetry (CV) was performed on a Zahner IM6 electrochemical workstation. CV curves were recorded at RT between 2 and 4.6 V (vs.  $\text{Li}^+/\text{Li}$ ) at a scan rate of 0.1 mV/s.

### Results and Discussion

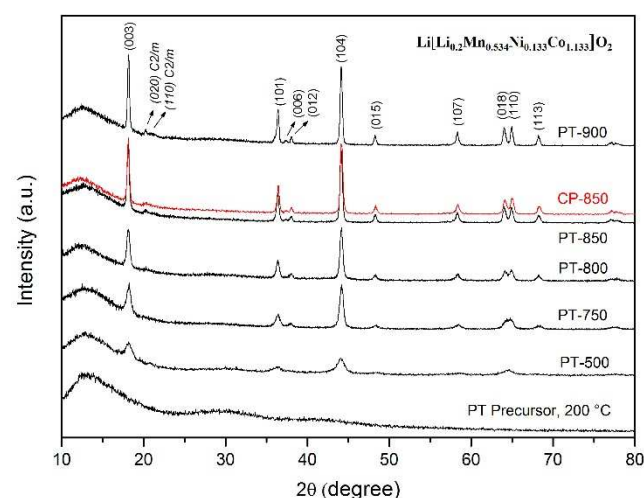


**Fig. 1** XRD patterns of the precursor and  $\text{Li}[\text{Li}_{0.2}\text{Mn}_{0.534}\text{Ni}_{0.133}\text{Co}_{0.133}]\text{O}_2$  layered oxides synthesized at temperatures from 500°C to 900°C.

The XRD patterns of the precursor and as-prepared  $\text{Li}[\text{Li}_{0.2}\text{Mn}_{0.534}\text{Ni}_{0.133}\text{Co}_{0.133}]\text{O}_2$  layered oxide calcined at temperatures ranging from 500 °C to 900 °C are shown in Fig. 1.

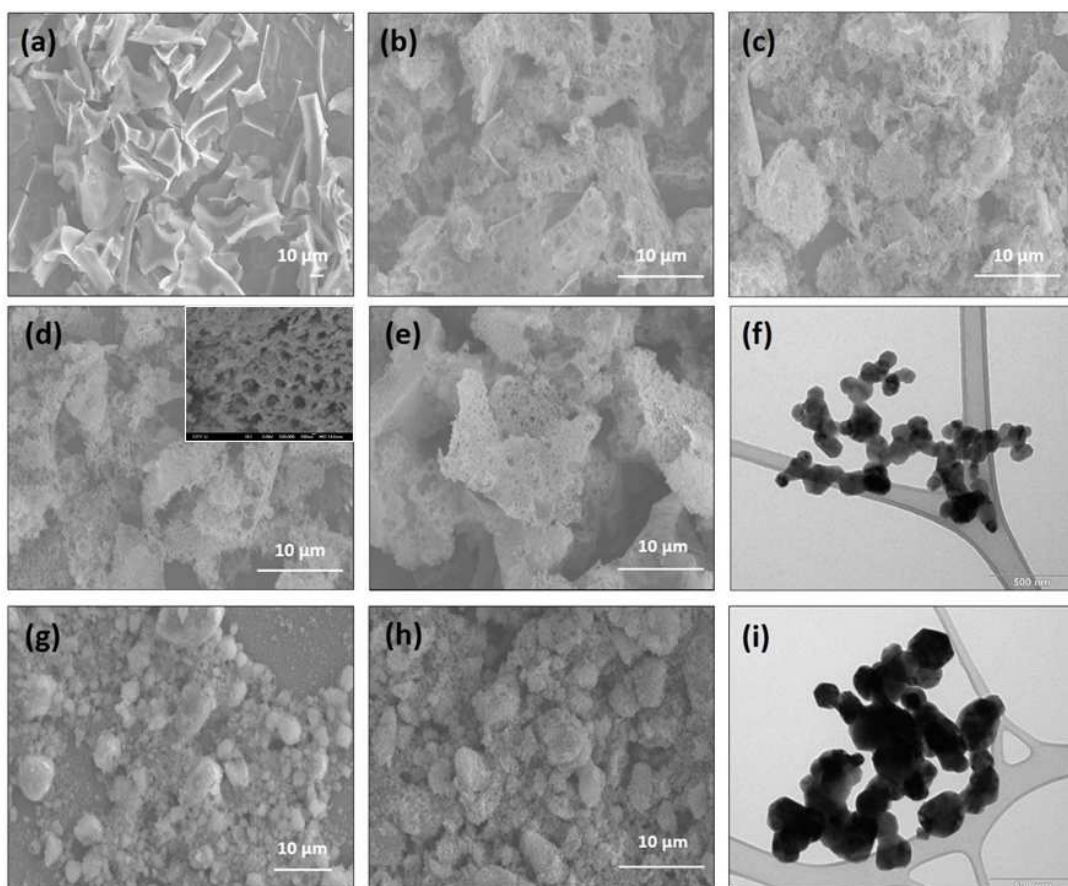


**Fig.2** Typical SEM images of (a) the polymer-based precursor of PT method, (b) PT-750, (c) PT-800, (d) PT-850, insert: FESEM image showing the pores, (e) PT-900, (g) the metal hydroxide precursor of CP method and (h) CP-850. (f) and (i) show the TEM image of PT-850 and CP-850, respectively.

5 All the strong reflections can be indexed based on a hexagonal  $\alpha$ -  
 $\text{NaFeO}_2$  structure (space group  $R\bar{3}m$ ). The peaks become sharper  
 and stronger with increasing calcination temperature. The weak  
 minor reflections between  $20^\circ$ - $25^\circ$  observed in the PT-850 and  
 PT-900 samples can only be indexed based on the monoclinic  
 $C2/m$  configuration, and are characteristic of the  $\text{LiMn}_6$  cation  
 10 ordering in the transition metal layers of  $\text{Li}_2\text{MnO}_3$ -like structures  
 $^{33-36}$ . As observed, the degree of splitting between the (006)/(102)  
 and (108)/(110) peaks increases with increasing calcination  
 temperature. When the calcination temperature is above  $850^\circ\text{C}$ , a  
 distinct and sharp peak-splitting is observed, indicating the  
 formation of a well-defined layered structure, and the undesirable  
 cation disordering between the lithium and metal ions is low  $^{37}$ .  
 The intensity ratio (R) of  $I_{003}/I_{104}$ , an indicator of the degree of  
 cation mixing  $^{38}$ , also increases from 0.672 for PT-750 to 0.879  
 20 for PT-900 (calculated after background removal). These results  
 mean that a higher calcination temperature promotes the  
 formation of a well-defined layered structure. No obvious  
 difference in peak position or peak intensity is observed between  
 sample PT-850 and CP-850.

25 SEM was performed to observe the morphology of the  
 precursor and the as-prepared  $\text{Li}[\text{Li}_{0.2}\text{Mn}_{0.534}\text{Ni}_{0.133}\text{Co}_{0.133}]\text{O}_2$   
 layered oxide samples using PT and CP methods. The obtained  
 SEM images are shown in Fig. 2. In the PT method, the polymer-  
 based precursor has an irregular shape with smooth surfaces and

30 sharp edges, with a particle size in the range of tens of  
 micrometers. The sizes of the secondary particle of the final  
 oxide powders are around  $10\ \mu\text{m}$ , and pores ( $\sim 100$ - $200\ \text{nm}$   
 across) formed between primary particles are observed on the  
 surface. TGA results of the precursor (see Figure S1 in the  
 35 Supporting Information) show that upon heating above  $400^\circ\text{C}$ ,  
 the polymer-precursor lost more than 80 wt% of its mass. This  
 mass loss is most likely caused by the decomposition of the  
 organic compounds and metal nitrates in the precursor, during  
 which a large amount of gases, such as  $\text{CO}$ ,  $\text{CO}_2$ , and  $\text{NO}_2$  are  
 40 released, along with the breakage of precursor particles  
 accompanying the formation of the highly porous structure. Such  
 porous structure may lead to an improved electrochemical  
 performance as the increased contact area between the oxide  
 powders and the electrolyte facilitates a faster Li-ion insertion-  
 45 extraction process. The EDS mapping results (see Figure S2)  
 confirms that in both the precursor and the final oxide powder,  
 the Ni, Co and Mn ions are homogeneously distributed. As for  
 the CP method, the morphologies of the metal hydroxide  
 precursor and the final product are similar, with sphere-like  
 50 secondary particles in the range of 1- $10\ \mu\text{m}$ .

TEM images of sample PT-850 and CP-850 are also shown in  
 Fig. 2. The particle size of PT-850 ( $\sim 50$ - $100\ \text{nm}$ ) is obviously  
 smaller than that of CP-850 ( $\sim 100$ - $300\ \text{nm}$ ). The  
 Brunauer-Emmett-Teller (BET) specific surface area of sample

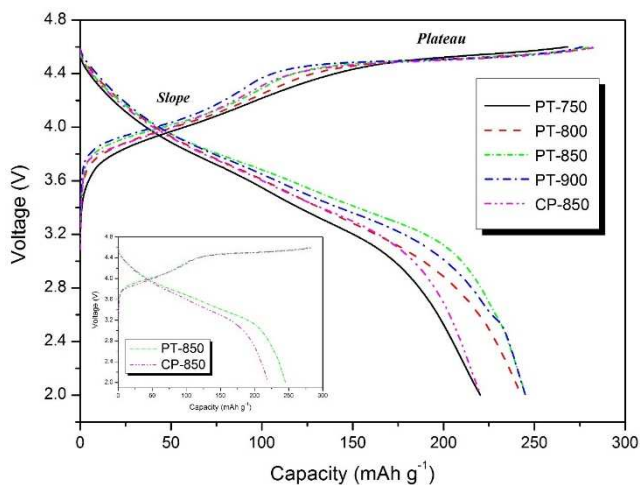


**Fig. 3** Initial charge-discharge curves of the  $\text{Li}[\text{Li}_{0.2}\text{Mn}_{0.534}\text{Ni}_{0.133}\text{Co}_{0.133}]\text{O}_2$  layered oxides calcined at different temperatures. The current density was set at  $15 \text{ mA g}^{-1}$ .

**Table 1**

The initial charge and discharge capacities, coulombic efficiency and irreversible capacity loss of the  $\text{Li}[\text{Li}_{0.2}\text{Mn}_{0.534}\text{Ni}_{0.133}\text{Co}_{0.133}]\text{O}_2$  samples.

	PT-750	PT-800	PT-850	PT-900	CP-850
Initial charge capacity ( $\text{mAh g}^{-1}$ )	268.4	283.9	282	276.5	285.3
Initial discharge capacity ( $\text{mAh g}^{-1}$ )	220.3	242.9	245.4	245.0	220.5
Irreversible capacity loss ( $\text{mAh g}^{-1}$ )	48.1	41.0	36.6	31.5	64.8
Coulombic efficiency (%)	82.1	85.6	87	88.6	77.3

PT-850 measured through nitrogen adsorption/desorption isotherms (see Figure S3) is  $10.63 \text{ m}^2 \text{ g}^{-1}$ . By contrast, the specific surface area of sample CP-850 is only  $2.325 \text{ m}^2 \text{ g}^{-1}$ . The small particle size and large surface area obtained by PT method are beneficial for faster Li-ion diffusion, and predict better electrochemical performance.

Fig. 3 shows the typical initial charge-discharge curves of the  $\text{Li}[\text{Li}_{0.2}\text{Mn}_{0.534}\text{Ni}_{0.133}\text{Co}_{0.133}]\text{O}_2$  samples synthesized at different temperatures at a current density of  $15 \text{ mA g}^{-1}$  in the voltage range of 2-4.6 V. As seen from the graph, the charge/discharge profiles are similar for all of the samples. The initial charge curve consists of a sloping a plateau region extending from 4 to 3V, which is characteristic of the  $x\text{Li}_2\text{MnO}_3 \cdot (1-x)\text{LiMO}_2$  type compounds. The sloped region corresponds to the  $\text{Li}^+$  extraction from the  $\text{LiMO}_2$  ( $M = \text{Mn, Ni and Co}$ ) component, accompanied by the oxidation of  $\text{Ni}^{3+}$  and  $\text{Co}^{3+}$  ions to  $\text{Ni}^{4+}$  and  $\text{Co}^{3.6+}$ , respectively<sup>39</sup>. While the plateau region above  $\sim 4.4 \text{ V}$  corresponds to the  $\text{Li}^+$  extraction from the  $\text{Li}_2\text{MnO}_3$  component. In the second and subsequent cycles, the plateau region in the charge curve disappears, indicating that this  $\text{Li}_2\text{MnO}_3$  activation process is irreversible (see Figure S4).

It has been shown that, although the Mn ions in  $\text{Li}_2\text{MnO}_3$  cannot be further oxidized (at room temperature), the removal of  $\text{Li}^+$  is enabled by the oxidation of  $\text{O}^{2-}$  ions, due to an overlap of the  $\text{Co}^{3+/4+} 3d$  band with the top of the  $\text{O}^{2-} 2p$  band, leading to the generation of oxygen vacancies and the formation of electrochemically active  $\text{MnO}_2$  phase and oxygen vacancies that

serve as sites for Li-ion insertion/extraction during the following discharge/charge processes, giving rise to the anomalous high rechargeable capacity of  $x\text{Li}_2\text{MnO}_3 \cdot (1-x)\text{LiMO}_2$  compounds. No obvious additional tail part is observed at the end of the first charge curves, suggesting that the amount of electrolyte decomposition in this 2-4.6 V voltage window is negligible.

The initial charge and discharge capacities, irreversible capacity loss, and coulombic efficiency of the samples are summarized in Table 1. Assuming complete Li-ion extraction from both  $\text{LiMO}_2$  and  $\text{Li}_2\text{MnO}_3$  components, the theoretical capacity of  $\text{Li}[\text{Li}_{0.2}\text{Mn}_{0.534}\text{Ni}_{0.133}\text{Co}_{0.133}]\text{O}_2$  would be  $377 \text{ mAh g}^{-1}$ . However, the actual reversible charge capacities obtained for sample PT-750, PT-800, PT-850, PT-900 and CP-850 are only 268.4, 283.9, 282, 276.5, and 285.3  $\text{mAh g}^{-1}$ , respectively, all significantly lower than the theoretical value. This implies that only part of the  $\text{Li}_2\text{MnO}_3$  component is activated during charge in the first cycle at a cut-off voltage of 4.6 V, which is also confirmed by the CV results, which will be discussed later. Overall, samples synthesized using PT method at and above 800 °C exhibits similar charge and discharge capacities of around 280  $\text{mAh g}^{-1}$  and 245  $\text{mAh g}^{-1}$ , respectively, as well as a high coulombic efficiency of around 87%. As for sample PT-750, a much lower charge/discharge capacity and a higher irreversible capacity loss are observed, possibly due to its poorly-formed layered structure suggested by XRD and hence a more sluggish reaction. Comparing sample PT-850 with CP-850, although they have almost identical XRD profile and initial charge/discharge voltage profiles, the discharge capacity and coulombic efficiency of CP-850 are significantly lower than that of PT-850.

To further understand the redox reaction processes of the obtained  $\text{Li}[\text{Li}_{0.2}\text{Mn}_{0.534}\text{Ni}_{0.133}\text{Co}_{0.133}]\text{O}_2$  powders, cyclic voltammetry (CV) tests were performed on samples PT-850 and CP-850 at a scan rate of  $0.1 \text{ mV s}^{-1}$  between 2 and 4.6 V for the first 5 cycles. As shown in Fig. 4, the two samples have similar CV curves. Two oxidation peaks are observed in the first charge process, one at  $\sim 4.1 \text{ V}$  and another at  $\sim 4.5 \text{ V}$ . The peak at  $\sim 4.1 \text{ V}$  is ascribed to the oxidation of  $\text{Ni}^{2+}$  to  $\text{Ni}^{4+}$  and  $\text{Co}^{3+}$  to  $\text{Co}^{3.6+}$ , corresponding to the extraction of  $\text{Li}^+$  from the  $\text{LiMO}_2$  structure. The other peak at  $\sim 4.5 \text{ V}$  is related to the Li-ion extraction from the  $\text{Li}_2\text{MnO}_3$  lattice accompanying with oxygen loss and possibly further oxidation of  $\text{Co}^{3.6+}$  to  $\text{Co}^{4+}$ . As observed, this peak at  $\sim 4.5 \text{ V}$  is still present in the following cycles. On the other hand, this peak almost disappears in the second cycle when the cut-off voltage is set as 4.8 V (see Figure S5). Thus it can be inferred that the  $\text{Li}_2\text{MnO}_3$  activation process is not easily completed in limited cycles at a cut-off voltage of 4.6 V<sup>40</sup>. The peak at  $\sim 4.1 \text{ V}$  becomes broader and shifts to lower voltages, indicating an enhanced chemistry related to the  $\text{Li}^+$  extraction from the  $\text{LiMO}_2$  structure, and further confirms the transformation of  $\text{Li}_2\text{MnO}_3$  into  $\text{MnO}_2$  at above 4.4 V in the first charge process. In the negative scan, there are also two reduction peaks at  $\sim 4.5 \text{ V}$  and  $\sim 3.8 \text{ V}$  in the first cycle, corresponding to the reduction of  $\text{Ni}^{4+}$  and  $\text{Co}^{4+}$  respectively. Two new broad redox peaks appear at around 2.9-3.3 V in the second cycle, and they are most likely associated with the redox reaction of  $\text{Mn}^{3+}/\text{Mn}^{4+}$ <sup>13,40</sup>, indicating the formation of  $\text{MnO}_2$  after the initial  $\text{Li}_2\text{MnO}_3$  activation process. The CV results agree well with the charge-discharge profiles.

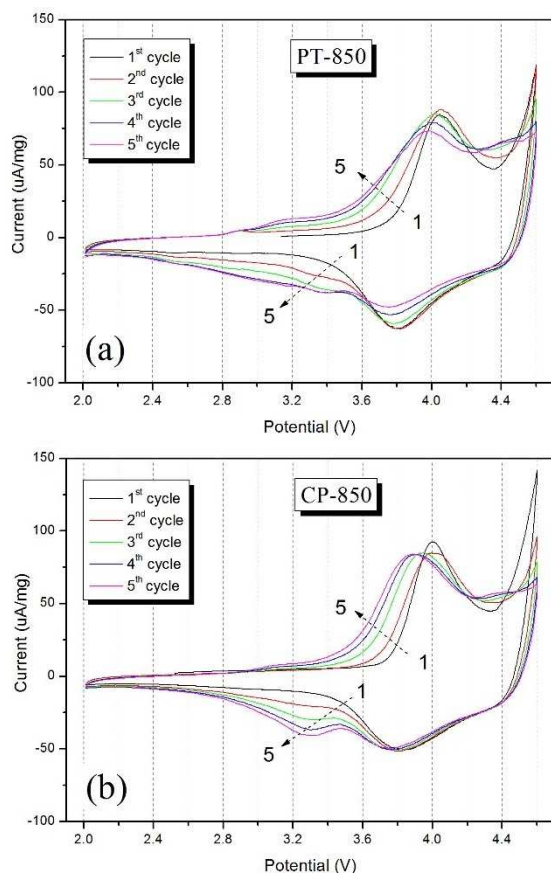


**Fig. 4** Cyclic voltammetry (CV) curves of sample PT-850 and CP-850 at a scan rate of  $0.1 \text{ mV s}^{-1}$  in the first five cycles.

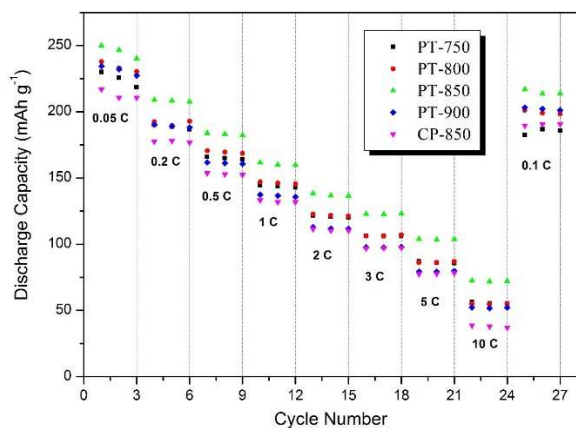


**Fig. 5** Rate performance of sample PT-850 and CP-850 from  $0.05 \text{ C}$  to  $1 \text{ C}$  between 2 and 4.6V.

Fig. 5 shows the rate performance of the layered oxides at  $15 \text{ mA g}^{-1}$  to  $3000 \text{ mA g}^{-1}$  ( $0.05 \text{ C}$  to  $10 \text{ C}$ ) between 2 V and 4.6 V. The PT-850 sample again displays the best performance, with a discharge capacity of 249.7, 216.8, 208.8, 183.9, 161.5, 138.3, 122.7, 103.9, and  $72.4 \text{ mAh g}^{-1}$  at the current density of 15, 30, 60, 150, 300, 600, 900, 1500 and  $3000 \text{ mA g}^{-1}$ , respectively, exceeding the capacities of sample CP-850 by about  $30 \text{ mAh g}^{-1}$  at all rates. This rate performance enhancement can be ascribed to the highly porous structures facilitating faster ion transport between the active particles and electrolyte.

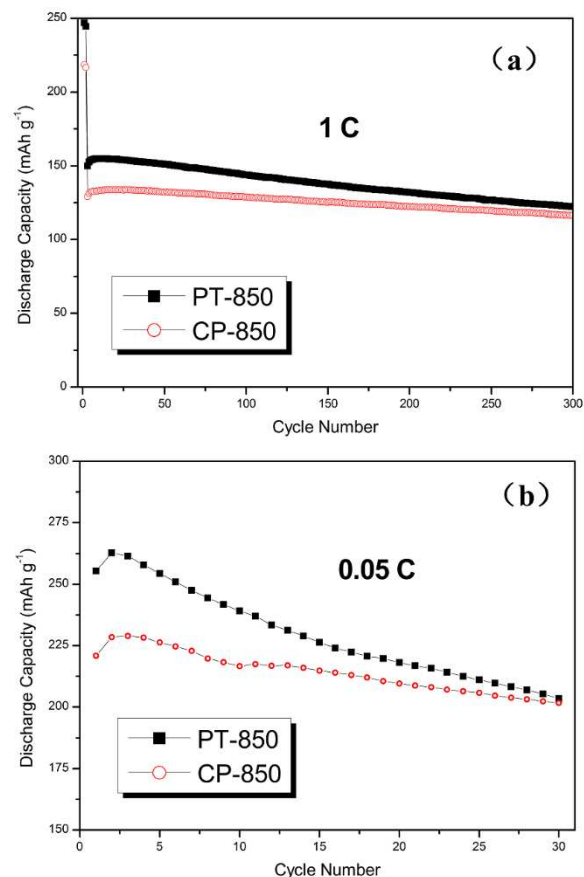


**Fig. 6** Cyclic performance of sample PT-850 and CP-850 at (a)  $300 \text{ mA g}^{-1}$  ( $1 \text{ C}$ ) and (b)  $15 \text{ mA g}^{-1}$  ( $0.05 \text{ C}$ ) between 2 and 4.6V.

Fig. 6 shows the cyclic performance of the as-synthesized samples at  $300 \text{ mA g}^{-1}$  ( $1 \text{ C}$ ) and  $15 \text{ mA g}^{-1}$  ( $0.05 \text{ C}$ ) between 2 V and 4.6 V. Although sample PT-850 exhibits the highest capacity at  $1 \text{ C}$  in the rate performance test, sample PT-800, PT-850 and PT-900 display similar cyclic performance, with a discharge capacity of 147, 150, and  $157 \text{ mAh g}^{-1}$  in the third cycle and a capacity retention value of approximately 81.1%, 82% and 79% after 300 cycles (with respect to the discharge capacity in the third cycle, see Figure S6). While for sample CP-850, only a discharge capacity of  $129.2 \text{ mAh g}^{-1}$  was obtained in the third cycle. Nonetheless, the capacity retention for CP-850 is approaching 90%. In the end of the 300<sup>th</sup> cycle. This effect is more significant at a low cycling current density, when cycled at  $15 \text{ mA g}^{-1}$  for 30 cycles, the capacity retention for PT-850 and CP-850 are 79.7% and 91.3%, respectively. The poor capacity retention of PT-850 is possibly caused by the enhanced side reaction between electrode and electrolyte, leading to Mn dissolution into the electrolyte and Mn valence state drop, which causes capacity loss<sup>41,42</sup>. Further investigation is needed to confirm this hypothesis.

## Conclusions

In summary, we have successfully synthesized high capacity porous  $\text{Li}[\text{Li}_{0.2}\text{Mn}_{0.534}\text{Ni}_{0.133}\text{Co}_{0.133}]\text{O}_2$  layered oxides using a novel polymer-thermolysis method. Their application as cathode materials for Li-ion batteries are evaluated. The best

electrochemical performance was obtained in the sample synthesized at 850 °C, with a high initial discharge capacity of 245.4 mAh g<sup>-1</sup>, a high initial coulombic efficiency of 87%, a reasonably good capacity retention value of approximately 81% after 300 cycles at 300 mA g<sup>-1</sup> and superior rate performance. Compared with the co-precipitation method, the polymer-thermolysis method produced samples with higher capacity and better rate performance thanks to the sample's very special nanoporous morphology formed by assembling of ultrafine nanoparticles. The results show that the polymer-thermolysis method could be a promising method for the synthesis of Li-rich metal oxide composite materials used as cathode materials for high energy Li-ion batteries.

## Acknowledgement

This work was financially supported by the National Natural Science Foundation of China (21001117) and the South University of Science and Technology of China through the Talent Development Starting Fund from the Shenzhen Government. The authors would also like to thank Dr. Hua Cheng and Ms Jie Zhang for their help in BET testing and analysis.

## Notes and references

<sup>a</sup> Department of Physics and Materials Science, City University of Hong Kong, Hong Kong SAR, PR China.

<sup>b</sup> School of Metallurgical Engineering, Hunan University of Technology

<sup>c</sup> Department of Materials Science & Engineering, South University of Science and Technology of China, Shenzhen, PR China. Fax: +86 88018944; Tel: +86 88018966; E-mail: [luzg@sustc.edu.cn](mailto:luzg@sustc.edu.cn) (LZG), [appchung@cityu.edu.hk](mailto:appchung@cityu.edu.hk) (CYC)

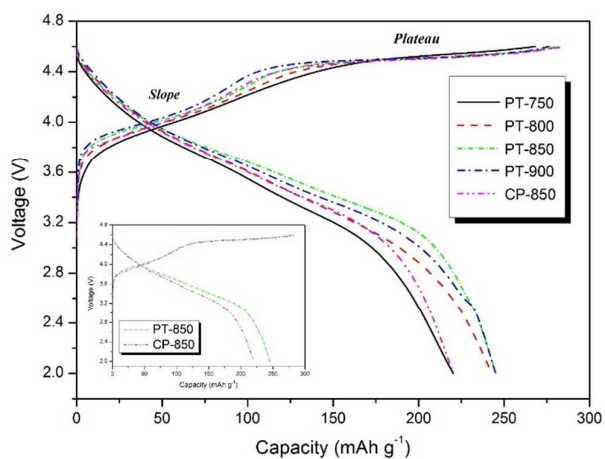
† Electronic Supplementary Information (ESI) available: [details of any supplementary information available should be included here]. See DOI: 10.1039/b000000x/

‡ Footnotes should appear here. These might include comments relevant to but not central to the matter under discussion, limited experimental and spectral data, and crystallographic data.

- J.-M. Tarascon and M. Armand, *Nature*, 2001, **414**, 359–367.
- M. Armand and J.-M. Tarascon, *Nature*, 2008, **451**, 652–657.
- A. Manthiram, *J. Phys. Chem. Lett.*, 2011, **2**, 176–184.
- R. Marom, S. F. Amalraj, N. Leifer, D. Jacob and D. Aurbach, *J. Mater. Chem.*, 2011, **21**, 9938–9954.
- M. M. Thackeray, C. Wolverton and E. D. Isaacs, *Energy Environ. Sci.*, 2012, **5**, 7854–7863.
- J. B. Goodenough and Y. Kim, *Chem. Mater.*, 2010, **22**, 587–603.
- V. Etacheri, R. Marom, R. Elazari, G. Salitra and D. Aurbach, *Energy Environ. Sci.*, 2011, **4**, 3243–3262.
- M. Hu, X. Pang and Z. Zhou, *J. Power Sources*, 2013, **237**, 229–242.
- K. Zaghbi, A. Mauger, H. Groult, J. Goodenough and C. Julien, *Materials*, 2013, **6**, 1028–1049.
- M. M. Thackeray, S.-H. Kang, C. S. Johnson, J. T. Vaughey, R. Benedek and S. A. Hackney, *J. Mater. Chem.*, 2007, **17**, 3112–3125.
- H. Yu and H. Zhou, *J. Phys. Chem. Lett.*, 2013, **4**, 1268–1280.
- J. Yan, X. Liu and B. Li, *RSC Adv.*, 2014, **4**, 63268–63284.
- Z. Lu and J. R. Dahn, *J. Electrochem. Soc.*, 2002, **149**, A815–A822.

- A. R. Armstrong, M. Holzapfel, P. Novák, C. S. Johnson, S.-H. Kang, M. M. Thackeray and P. G. Bruce, *J. Am. Chem. Soc.*, 2006, **128**, 8694–8698.
- N. Yabuuchi, K. Yoshii, S.-T. Myung, I. Nakai and S. Komaba, *J. Am. Chem. Soc.*, 2011, **133**, 4404–4419.
- Y. W. Denis and K. Yanagida, *J. Electrochem. Soc.*, 2011, **158**, A1015–A1022.
- A. van Bommel and J. R. Dahn, *Electrochem. Solid-State Lett.*, 2010, **13**, A62–A64.
- H. Yu, Y. Wang, D. Asakura, E. Hosono, T. Zhang and H. Zhou, *RSC Adv.*, 2012, **2**, 8797–8807.
- M. G. Kim, M. Jo, Y.-S. Hong and J. Cho, *Chem. Commun.*, 2009, 218–220.
- G.-Z. Wei, X. Lu, F.-S. Ke, L. Huang, J.-T. Li, Z.-X. Wang, Z.-Y. Zhou and S.-G. Sun, *Adv. Mater.*, 2010, **22**, 4364–4367.
- Z. Lu, L. Y. Beaulieu, R. A. Donaberge, C. L. Thomas and J. R. Dahn, *J. Electrochem. Soc.*, 2002, **149**, A778–A791.
- Y. Wang, N. Sharma, D. Su, D. Bishop, H. Ahn and G. Wang, *Solid State Ion.*, 2013, **233**, 12–19.
- X. Yang, X. Wang, G. Zou, L. Hu, H. Shu, S. Yang, L. Liu, H. Hu, H. Yuan, B. Hu, Q. Wei and L. Yi, *J. Power Sources*, 2013, **232**, 338–347.
- J. Li, L. Wang, L. Wang, J. Luo, J. Gao, J. Li, J. Wang, X. He, G. Tian and S. Fan, *J. Power Sources*, 2013.
- J. Shojan, V. R. Chitturi, L. Torres, G. Singh and R. S. Katiyar, *Mater. Lett.*, 2013.
- O. Toprakci, H. A. K. Toprakci, Y. Li, L. Ji, L. Xue, H. Lee, S. Zhang and X. Zhang, *J. Power Sources*, 2013.
- C. Yu, G. Li, X. Guan, J. Zheng and L. Li, *J. Alloys Compd.*, 2012, **528**, 121–125.
- S. J. Shi, J. P. Tu, Y. Y. Tang, Y. X. Yu, Y. Q. Zhang, X. L. Wang and C. D. Gu, *J. Power Sources*, 2013, **228**, 14–23.
- C. Ghanty, S. Chatterjee, R. N. Basu and S. B. Majumder, *J. Electrochem. Soc.*, 2013, **160**, A1406–A1414.
- R. N. Das, *Mater. Lett.*, 2001, **47**, 344–350.
- W. He, J. Qian, Y. Cao, X. Ai and H. Yang, *RSC Adv.*, 2012, **2**, 3423–3429.
- Y. Jiang, Z. Yang, W. Luo, X.-L. Hu, W.-X. Zhang and Y.-H. Huang, *J. Mater. Chem.*, 2012, **22**, 14964–14969.
- M. M. Thackeray, S.-H. Kang, C. S. Johnson, J. T. Vaughey and S. A. Hackney, *Electrochem. Commun.*, 2006, **8**, 1531–1538.
- J. Bréger, M. Jiang, N. Dupré, Y. S. Meng, Y. Shao-Horn, G. Ceder and C. P. Grey, *J. Solid State Chem.*, 2005, **178**, 2575–2585.
- K. A. Jarvis, Z. Deng, L. F. Allard, A. Manthiram and P. J. Ferreira, *Chem. Mater.*, 2011, **23**, 3614–3621.
- H. Koga, L. Croguennec, P. Manessiez, M. Ménétrier, F. Weill, L. Bourgeois, M. Duttine, E. Suard and C. Delmas, *J. Phys. Chem. C*, 2012, **116**, 13497–13506.
- T. A. Arunkumar, E. Alvarez and A. Manthiram, *J. Electrochem. Soc.*, 2007, **154**, A770–A775.
- K. M. Shaju, G. V. Subba Rao and B. V. R. Chowdari, *Electrochimica Acta*, 2002, **48**, 145–151.
- T. A. Arunkumar, Y. Wu and A. Manthiram, *Chem. Mater.*, 2007, **19**, 3067–3073.
- H. Yu, H. Kim, Y. Wang, P. He, D. Asakura, Y. Nakamura and H. Zhou, *Phys. Chem. Chem. Phys.*, 2012, **14**, 6584–6595.
- J. Zheng, M. Gu, J. Xiao, P. Zuo, C. Wang and J.-G. Zhang, *Nano Lett.*, 2013, **13**, 3824–3830.
- X. Lin, J. Park, L. Liu, Y. Lee, A. M. Sastry and W. Lu, *J. Electrochem. Soc.*, 2013, **160**, A1701–A1710.

## Facile synthesis of porous Li-rich layered $\text{Li}[\text{Li}_{0.2}\text{Mn}_{0.534}\text{Ni}_{0.133}\text{Co}_{0.133}]\text{O}_2$ as high-performance cathode materials for Li-ion batteries



Porous Li-rich layered  $\text{Li}[\text{Li}_{0.2}\text{Mn}_{0.534}\text{Ni}_{0.133}\text{Co}_{0.133}]\text{O}_2$  was successfully prepared by a facile polymer-thermolysis method and exhibited superior electrochemical performance as cathode materials for lithium ion batteries.